Arch. Mech., 44, 1, pp. 69–84, Warszawa 1992

Multiaxial low cycle fatigue damage of an austenitic and two ferritic steels at 20°C and 600°C

V. DOQUET (PALAISEAU) and J. WEISS (EVRY)

COMBINED and sequential tension and torsion tests have been performed on a 316 stainless steel, a mild steel and a 12% chromium steel at 20°C and 600°C. The analysis of the fatigue lifes obtained is supported by observations of crack initiation and propagation mechanisms, that also enables interpretation of history effects appearing in damage cumulation when tensile and torsional loading alternate.

1. Introduction

CONCERNING fatigue damage, many people have in mind the classical scheme according to which fatigue life divides into stage I—covering crack initiation and growth along maximum shear strain planes—and stage II, during which the main crack propagates perpendicular to the first principal stress.

But these notions were derived from uniaxial tensile tests exclusively. The results presented in this paper show that they are not easily generalized to high temperature or multiaxial loading situations. Moreover, the fatigue damage cumulation rules that have been developed to evaluate the residual life of components subjected to uniaxial loadings consider damage as a scalar entity. It is shown that such models fail under multiaxial loading where damage anisotropy plays an essential role.

2. Materials and experimental procedure

Three materials: a 316 stainless steel, a mild steel and a 12% chromium steel were investigated. Their chemical composition and mechanical properties are given in Table 1 and 2.

Table 1. Chemical composition of the materials (weight %).

Material	C	N	Ni	Cr	Mo	Mn	Cu	Si	Al	P	S
316stainless steel	0.034	0.068	12.45	17.3	2.52	1.85	0.2	0.53	–	0.029	0.004
Mild steel	0.049	0.002	0.02	0.013	–	0.188	0.013	0.009	0.064	0.014	0.017
12% Chromium steel	0.103	0.043	2.82	11.9	1.7	0.78	–	0.26	–	0.028	0.002

Combined and sequential tension and torsion tests were carried out, either at room temperature or at 600°C on 1.5 mm thick tubular specimens with an outer diameter of 19.5 mm. During these tests, both the longitudinal and shear strains of the specimens: $\varepsilon = (\Delta\varepsilon/2)\cos\omega t$, $\gamma = (\Delta\gamma/2)\cos(\omega t + \phi)$ and their phase difference ϕ were controlled. Depending on the value of ϕ, (0 or 90 degrees), proportional or non-proportional loading

Table 2. Mechanical properties of the materials.

Material	Yield stress (MPa)	Ultimate tensile stress (MPa)	Elongation (%)
316 stainless steel	$\sigma_{0.2\%} = 321$	592	50
Mild steel	$\sigma_u = 263$ $\sigma_l = 210^*$	316	37
12% chromium steel	$\sigma_{0.2\%} = 828$	1006	18

σ_u— upper yield stress
σ_l— lower yield stress

was imposed. The ratio between shear and longitudinal strain amplitudes: ($\lambda' = \Delta\gamma/\Delta\varepsilon$) ranged from 0 (pure tension) to ∞ (pure torsion). The strain rates were kept approximately at the order of $10^{-3}s^{-1}$. Failure was defined as a 15 to 20% drop in shear or axial stress amplitude. Von Mises stress or strain equivalent amplitudes used to present test results are defined in the most general case by

$$\Delta\sigma_{\text{eq Mises}} = \underset{t_1}{\text{Max}}\ \underset{t_2}{\text{Max}}(J_2(\sigma(t_1) - \sigma(t_2))),$$

$$\Delta\sigma_{\text{eq Mises}} = \underset{t_1}{\text{Max}}\ \underset{t_2}{\text{Max}}(J_2(\varepsilon(t_1) - \varepsilon(t_2))).$$

In the present case, these equivalent amplitudes are obtained as the diameters of the circumscribing circles the stress and strain paths drawn in the planes $(\sigma, \sqrt{3}\tau)$, $(\varepsilon, \gamma/\sqrt{3})$. The equivalent plastic strain range, $\Delta\varepsilon_{p\,\text{eq Mises}}$ is derived by the same procedure from the plot of $1/\sqrt{3}(\gamma - \tau/\mu)$ versus $(\varepsilon - \sigma/E)$.

3. Results and discussion

3.1. Combined tension and torsion tests

3.1.1. Tests carried out at room temperature

a. Cyclic behaviour

The cyclic stress-strain curves of 316 stainless steel are plotted in Fig. 1, together with its monotonic tensile curve. Some test results are taken from Refs. [1] and [2]. It can be observed that cyclic hardening — already important under uniaxial loading — is tremendously enhanced by multiaxial non-proportional loadings. For a given equivalent plastic strain range, the amount of additional hardening is governed by the λ' ratio and reaches a maximum of 72% for a value of this parameter close to $\sqrt{3}$.

Observations of intense slip bands emerging at the free surface of specimens were performed and the mean number of octahedral slip planes activated per grain — for a given equivalent strain amplitude — was measured (see Table 3). It appears that the number of active slip systems is increased by non-proportional loadings. The strong interactions between the various active slip systems raise the internal stresses and are responsible for the additional hardening observed.

An account of the way micromechanical modelling may successfully be employed to describe this phenomenon — beyond the scope of this paper — can be found in [3] and [4].

Figure 2 shows the cyclic stress-strain curves of mild steel (using Tresca equivalents). In spite of some scatter, it can be seen that multiaxial proportional loading has no definite effect on the cyclic behaviour of this ferritic steel, whereas additional hardening under

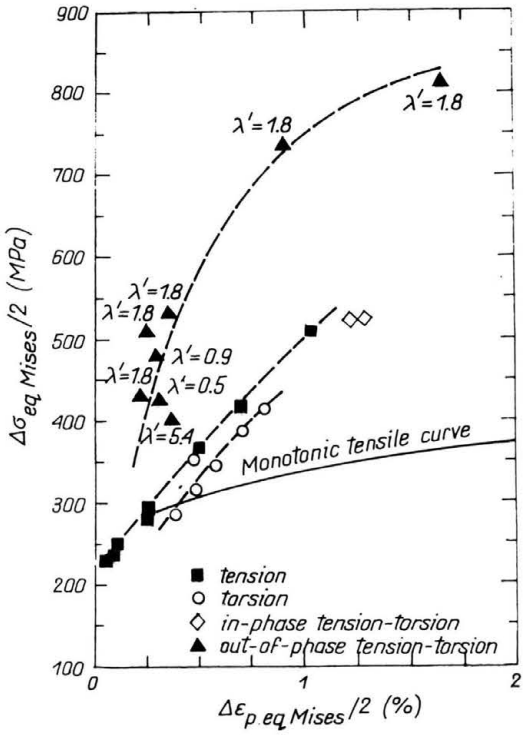

FIG. 1. Cyclic stress-strain curves of 316 stainless steel.

Table 3. Quantitative results of SEM observations performed on the outer surface of 316 stainless steel specimens.

Test	Tension-compression	Out-of-phase tension-torsion		
λ'	0	5.4	0.9	1.8
$\frac{\Delta\sigma_{eq\ Mises}}{2}$	309MPa	403 MPa	480 MPa	530 MPa
Number of slip plane traces per grain(n)	1.25	1.9	1.6	1.7
Mean interslip band spacing(i)	3.1 μm	4.3 μm	4.7 μm	5.5 μm
$n(\frac{d}{i})^*$	20	22	17	15.5

* d — grain size

out-of-phase loading is less important than in the austenitic stainless steel: the equivalent stress response under out-of-phase tension and torsion is at maximum 40% higher than under uniaxial loading.

The third material investigated, the 12% chromium steel does not exhibit additional hardening effects at all [5]. An attempt to explain the occurrence — or absence — of extra hardening in a material under non-proportional loadings by certain microstructural features can be found [6] and [4].

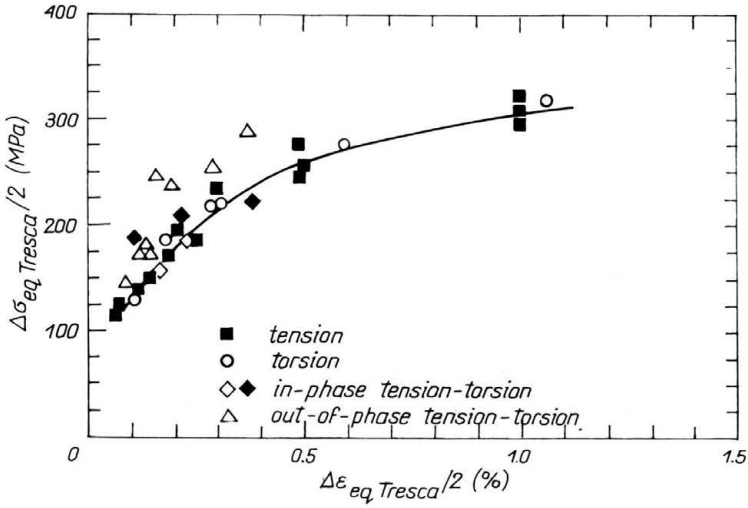

FIG. 2. Cyclic stress-strain curves of mild steel.

b. Fatigue lifes

The numbers of cycles to failure obtained during tension-compression, reversed torsion and combined tension and torsion tests are plotted versus the equivalent strain amplitudes applied in Figs. 3 and 4 for 316 stainless steel and mild steel, respectively.

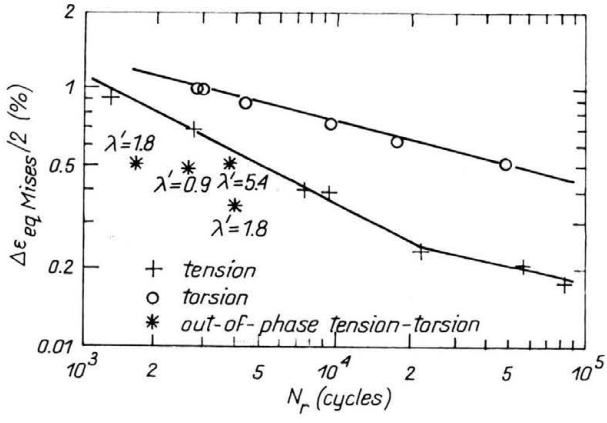

FIG. 3. Fatigue life of 316 stainless steel as a function of the equivalent strain amplitude.

The first striking result is that, for a given equivalent strain range, the fatigue life under reversed torsion is much larger — up to a factor of ten in stainless steel — than under tension-compression. Data concerning other materials of widely different mechanical properties [7] show that this is a rather general phenomenon that will be discussed further.

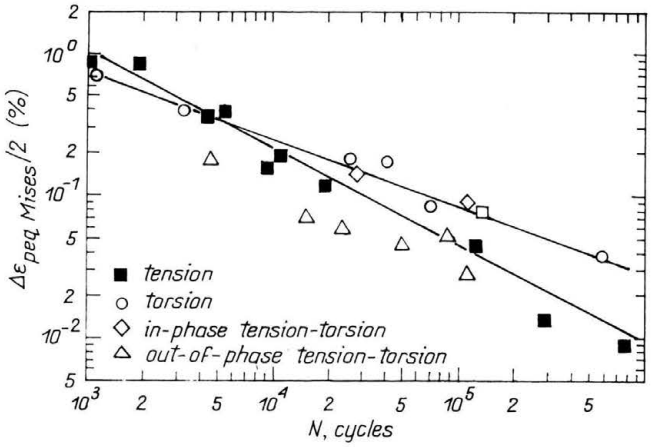

FIG. 4. Fatigue life of mild steel as a function of the equivalent stress amplitude.

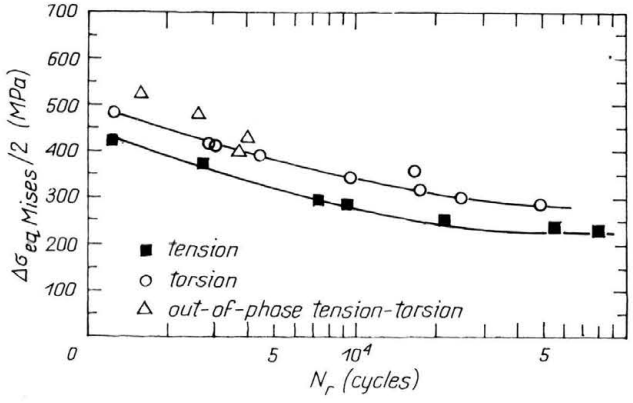

FIG. 5. Fatigue life of 316 stainless steel as a function of the equivalent stress amplitude.

It can be seen in Fig. 3 that for a given equivalent strain range, the endurance of 316 stainless steel under out-of-phase tension and torsion is largely dependent on the λ' ratio. The fatigue life reduction varies in the same sense as the amount of additional hardening and reaches a factor of 5 — compared to tension test results — when λ' equals 1.8, that is for the maximum hardening rate. It is worth mentioning however that the results obtained under the different loading modes do not unify when fatigue lifes are plotted versus the equivalent stress amplitude (Fig. 5).

Figure 4 shows that, as well as additional hardening, fatigue life reductions induced by non-proportional loadings are less important in mild steel: the endurance of specimens tested under out-of-phase tension and torsion is two to three times less than under tension-compression.

c. Crack propagation

Many authors have already observed a transition occurring in several materials above a given shear strain range in the crack propagation mode under reversed torsion. (See for example [8]). For low strain amplitudes a mode I helicoidal crack develops at 45° to the specimen's axis and grows almost isolated. At intermediate level, damage is more evenly distributed, the main crack still lies in a principal plane but seems to have developed by linking of longitudinal and transversal microcracks (Fig. 6a). At higher amplitudes, the major crack propagates in a longitudinal or transversal plane and may eventually branch, but very late in the fatigue life (Fig. 6b). At these high strain levels the network of longitudinal and transversal microcracks left by the initiation stage is very dense and there is a growing consensus to attribute the apparent Mode (II + III) crack propagation to collinear microcrack linking [9, 10].

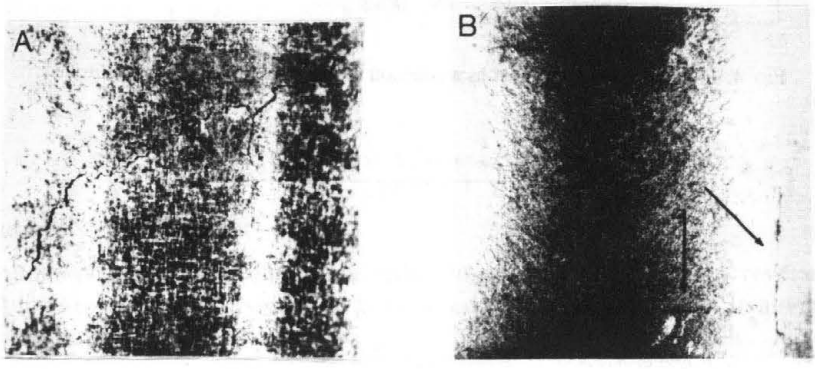

FIG. 6. Direction of main cracks in mild steel specimens submitted to reversed torsion.
a) $\Delta\gamma/2 = 0.158\%$, $N_F = 581\,000$ cycles;
b) $\Delta\gamma = 0.43\%$, $N_F = 41\,800$ cycles. (The loading axis is vertical, the magnification is ×8).

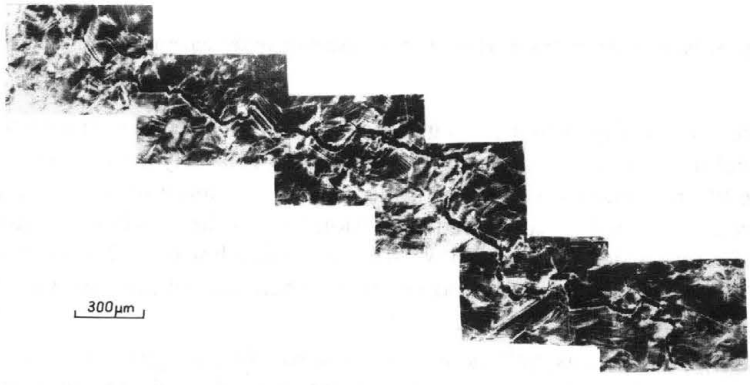

FIG. 7. Aspect of a crack developed under out-of-phase tension and torsion in 316 stainless steel ($\lambda' = 1.8$).

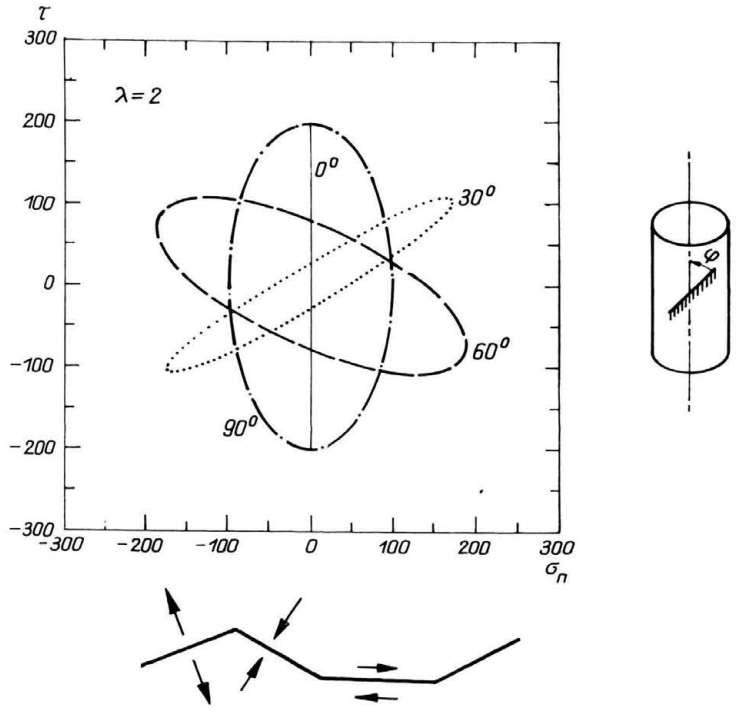

FIG. 8. Stress path undergone by facets inclined at 0, 30, 60 and 90 degrees during out-of-phase tension and torsion for a ratio between shear and longitudinal amplitude $\Delta\tau/\Delta\sigma$ equal to 2.

However, the parameters that control the transition from Mode I to apparent Mode (II + III) still have to be investigated. Furthermore, very few experimental data about the kinetics of shear-mode crack propagation are available [11].

When tension and torsion are combined, and especially out-of-phase, crack propagation becomes very difficult to analyze since the crack paths do not generally follow a simple direction characterized either by maximum shear stress range or normal stress range. But, as is illustrated in Fig. 7, cracks are very distorted. Each portion of the crack being submitted to a specific loading path that depends on its orientation (see Fig. 8a) portions are closed while others are opened and others sheared (Fig. 8b). In these conditions, propagation is probably not easy, especially in a hardened material. This suggests that the detrimental effect of non-proportional loadings might lie rather in a shortened crack initiation period than in an accelerated crack propagation stage.

d. Crack initiation

Crack initiation in 316 stainless steel is essentially transgranular. Systematic observations of microcracks were performed on both the free surface and a longitudinal cut of specimens so as to obtain histograms showing the angular repartition of damage around the axis. These histograms were analyzed thanks to 3-dimensional calculations of the shear and normal strain range undergone by any facet [4].

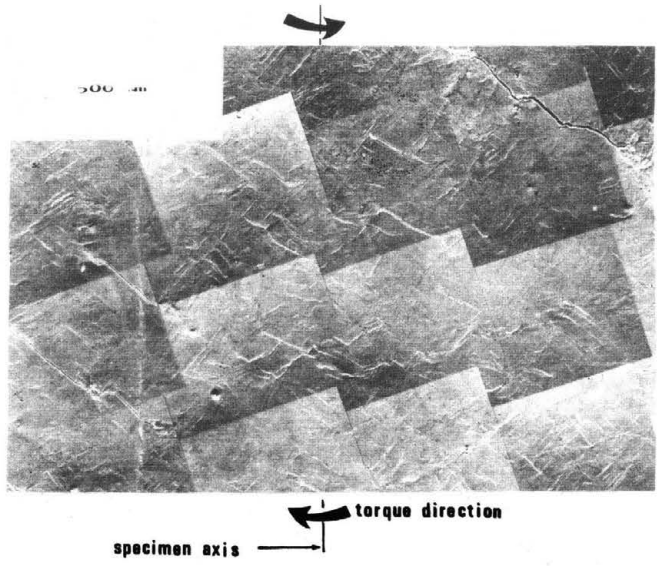

FIG. 9. (Taken from Ref. [15]). Microcracks distribution at the surface of a 12% chromium steel specimen submitted to tension-compression ($\Delta\sigma/2$ = 759 MPa, $\Delta\varepsilon/2$ = 0.53%) with a superimposed static torque (τ = 57 MPa).

It appears that the favourite planes for transgranular crack initiation are those undergoing the maximum shear strain range, but that the normal stress acting on these planes also has a favourable or inhibitory influence. The latter point is illustrated by Fig. 9 showing the repartition of microcracks at the surface of a 12% chromium steel specimen submitted to tension-compression with a superimposed static torque. Although this torque was not very important compared to the tensile stress (τ = 59 MPa, $\Delta\sigma/2$ = 759 MPa), the tensile or compressive stress it generated on facets inclined by $\pm 45°$ was sufficient to induce damage asymmetry.

This suggest that in the case of reversed torsion, the absence of normal stress on the facets where microcracks initiate (Fig. 10b) might have a retardation effect on crack initiation. This could explain the much longer fatigue lifes observed under reversed torsion, especially for small strain amplitudes, that is for life-times essentially spent in the crack initiation stage.

Since crack initiation in 316 stainless steel took place along intense slip bands, the impact of non-proportional loading on strain localization was studied, and the mean distance between intense slip bands was measured on the outer surface of specimens submitted to equivalent strain range (see Table 3). It appeared that this distance increased with the equivalent stress range as if strain localization became more difficult when the material hardened (Fig. 11).

This point conflicts with the conclusions usually drawn from uniaxial tests but is is consistent with similar observations by CLAVEL *et al.* [12] on waspalloy specimens tested

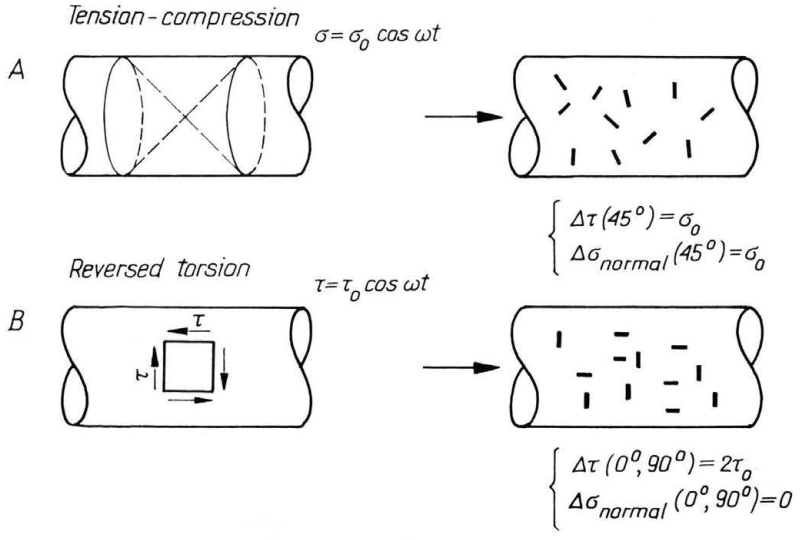

FIG. 10. Maximum shear strain directions and resulting microcrack distribution under a) tension-compression and b) reversed torsion.

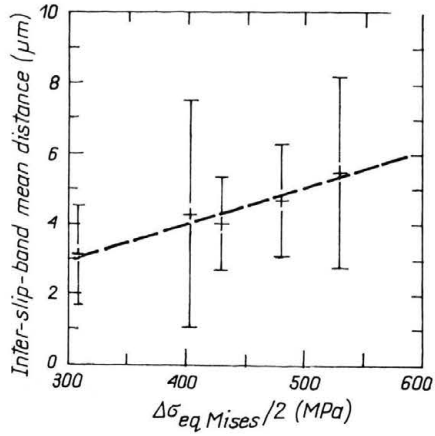

FIG. 11. Slip band spacing in 316 stainless steel as a function of the equivalent stress amplitude.

in tension and torsion. A possible explanation might be that since — for a given equivalent strain range — there are more active slip planes per grain, each of these has less deformation to carry and thus produces more distant slip traces. Taking the multiplicity of slip into account, the mean number of intense slip band per grain may be roughly estimated by: $(n \cdot d)/i$ (where n is the number of slip planes activated per grain, i the inter-slip-band distance and d the grain size). The fact that this parameter does not exhibit very significant variation from one specimen to another (see Table 3) supports the idea

of „strain redistribution". But the increase in slip band spacing might also be the sign of more pronounced strain localization that could be responsible for early crack initiation, and could thus explain the important fatigue life reductions observed.

The impact of non-proportional loadings on the crack initiation process in mild steel is quite different. In this material cracks initiate along slip bands as well as along grain boundaries. The rate of intergranular cracking — defined as the ratio of the summed length of intergranular microcracks to the summed length of all microcracks observed — measured on various specimens is reported in Table 4. It appears that multiaxial and especially non-proportional loading promote intergranular crack initiation.

Table 4. Quantitative analysis of crack initiation modes in mild steel.

Loading mode	$\frac{\Delta\varepsilon_{eqMises}}{2}$ (%)	$N_{Failure}$ (cycles)	Rate of intergranular cracking (%)	Rate of transgranular cracking (%)
Tension	0.18	17 471	26	74
Torsion	0.25	41 788	45	55
In-phase tension	0.14	114 574	35	65
and torsion	0.22	28 471	45	55
Out-of-phase	0.145	15 432	68	28
tension and torsion	0.28	4 610	81	19

This phenomenon is not clearly understood yet. Moreover, the preferred orientations for intergranular crack initiation were measured but no correlation could be found between these directions and any macroscopic mechanical parameter. This phenomenon clearly has to be analyzed at a microscopic scale. Such a micromechanical study was performed by LIM [13] on nickel specimens in uniaxial fatigue. He concluded that intergranular crack initiation is favoured when the out-of-surface differential component of Burgers vectors acting in each neighbouring grain is important. The probability for this condition to be realized might be increased under non-proportional loading because of slip multiplicity.

3.1.2. Tests carried out at 600°C

a. Cyclic behaviour

The additional hardening induced by non-proportional loading in 316 stainless steel at 600°C is less important that at room temperature: for a λ' ratio close to $\sqrt{3}$, the increase in the equivalent stress amplitude due to out-of-phase tension and torsion is around 32%. Easier cross-slip and dynamic recovery may explain this behaviour [14].

b. Fatigue lifes

The fatigue lifes observed in 316 stainless steel at 600°C under tension-compression, reversed torsion, in phase and out of phase tension and torsion are compared in Fig. 12 to the fatigue lifes measured at room temperature. It appears that high temperature loading produces very important fatigue life reductions whatever the loading mode, but that this detrimental effect disappears provided that the test is carried out under vacuum.

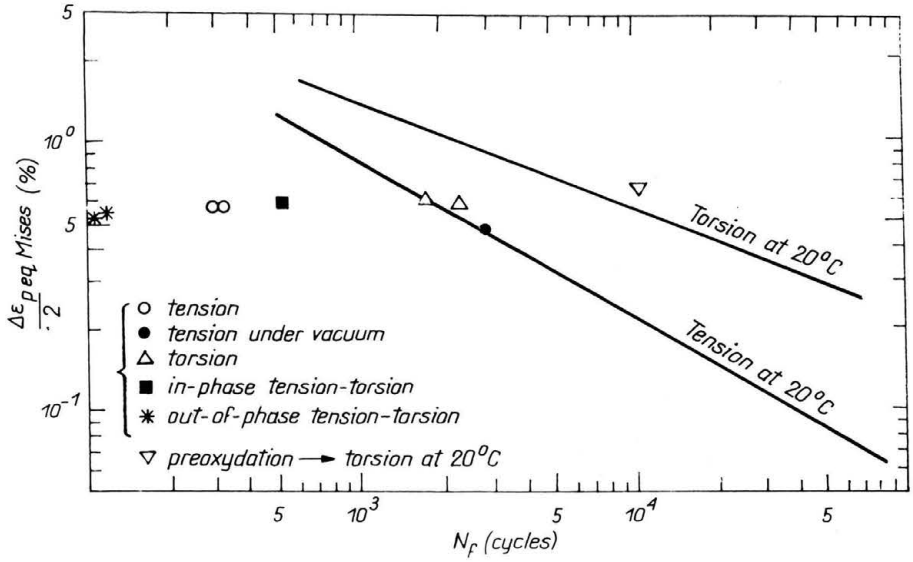

FIG. 12. Comparison of fatigue lifes of 316 stainless steel at 600°C and at 20°C.

This clearly indicates that environment effects are involved. When 316 stainless steel is submitted to air environment at 600°C, a chromium oxyde passivating film (Cr_2O_3) forms. But the fact that the fatigue life under reversed torsion at room temperature is unchanged by a 3-hour preoxydation at 600°C (see Fig. 12) shows that this chromium oxyde layer does not play any mechanical role in itself. Fatigue life reductions thus result from the simultaneous action of load and environment.

c. Crack initiation and growth

High temperature upsets the damage process: although crack initiation is still transgranular, it takes place under the action of the opening stress instead of the shear stress. Under tension-compression (Fig. 13a) cracks initiate perpendicular to the tensile axis, as if stage I would not exist anymore. Under reversed torsion (Fig. 13b) and in phase tension and torsion (Fig. 13c), microcrack orientations also coincide with the principal planes. It is worth mentioning that this drastic change in crack initiation mode did not happen in the specimen tested at 600°C under vacuum. It is thus related to the oxyde formation. Figure 14 shows that microcracks are surrounded by white oxyde clusters, that turn out to be iron oxyde on the outer surface, and mixed iron and chromium oxyde in the underlying layer.

It seems that cyclic loading brakes the chromium oxyde film — thus letting oxygen diffuse to the metal surface — and that slip bands play the role of diffusion channels for oxygen, thus leading to internal oxydation.

But the way brittle oxydes interfere with crack initiation is not fully explained for the time being. As concerns crack propagation, high temperature does not produce any modification. In particular under reversed torsion, the main crack still develops in a longitudinal or transversal plane by microcrack linking, although microcracks are not collinear with these directions (see Fig. 15).

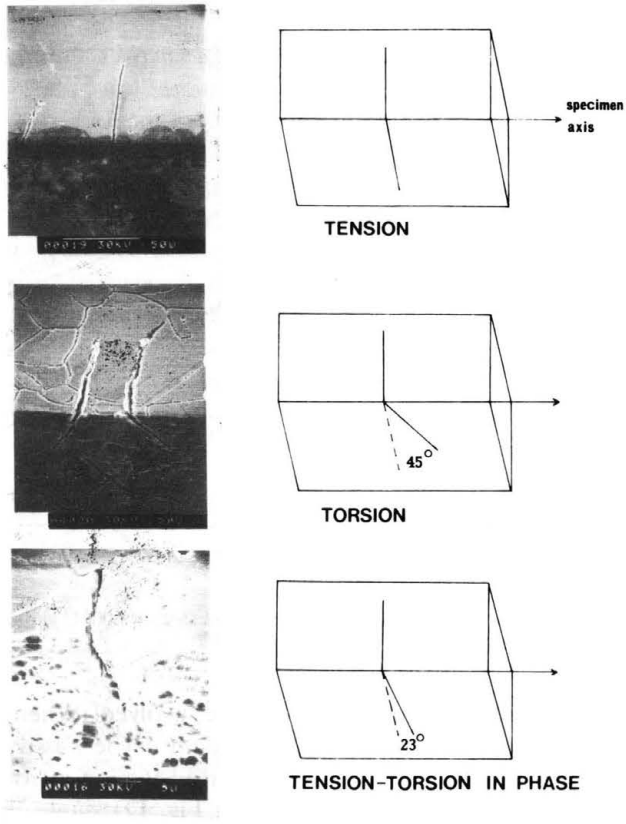

FIG. 13. Directions of cracks initiated at 600°C in 316 stainless steel under a) tension-compression, b) reversed torsion, c) in-phase tension and torsion.

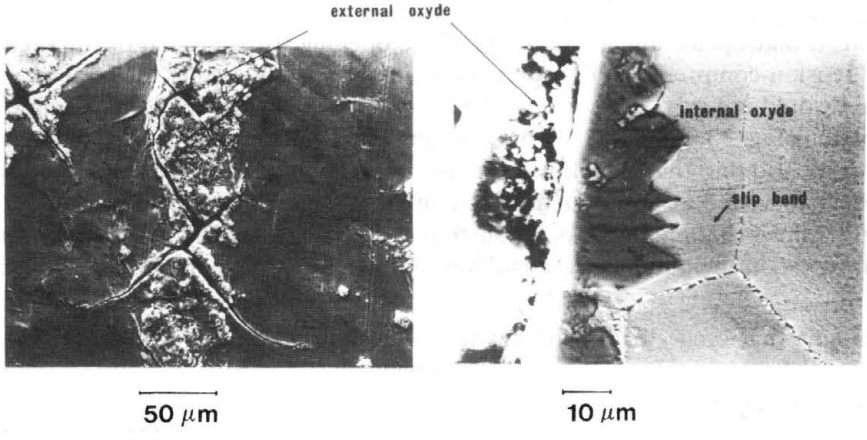

FIG. 14. The different oxyde layers formed in 316 stainless steel during cyclic loading at 600°C.

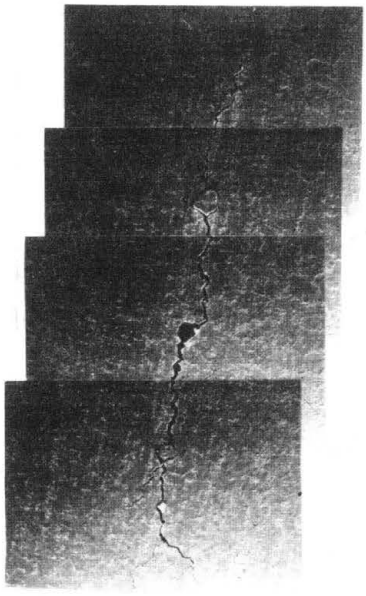

FIG. 15. Microcrack linking and crack growth at 600°C under reversed torsion in 316 stainless steel.

3.2. Sequential tension and torsion tests

Such tests have been performed by ROBILLARD [5] on 12% chromium steel at room temperature. After a given number of tension-compression cycles ($\Delta\varepsilon/2 = 0.5\%$), the specimens were submitted to reversed torsion ($\Delta\gamma/2 = 0.85\%$) until failure, or, on the contrary, reversed torsion was applied first, and tension-compression afterwards. The reference fatigue lifes for $\Delta\varepsilon/2 = 0.5\%$ and $\Delta\gamma/2 = 0.85\%$ had been determined previously. The percentage of remaining life measured under the second loading mode are plotted in Fig. 16a versus the fractions of fatigue life already spent under the first loading sequence. A line represents the Miner linear damage cumulation rule,

$$\frac{N_1}{NR_1} + \frac{N_2}{NR_2} = 1.$$

It appears that damage cumulation is asymmetrical and depends on the order of loading sequences. If tension-compression is applied first, and even if $N_1/(NR_1)$ is already important, specimens retain almost all their capacity to support torsion loading. On the contrary, torsion cycling efficiently reduces the residual life under tension-compression.

If we compare these results with those of similar tests carried out at somewhat higher strain levels ($\Delta\varepsilon/2 = 0.8\%$, $N_R = 300$ cycles $\Delta\gamma/2 = 1.38\%$, $N_R = 2000$ cycles) on 316 stainless steel at 600°C (Fig. 16b) we discover that the damage cumulation tendency is exactly the opposite. Tensile damage very efficiently reduces the fatigue life under torsion, whereas torsion damage, up to a certain value of $N_1/(NR_1)$, does not influence the fatigue life under tension-compression.

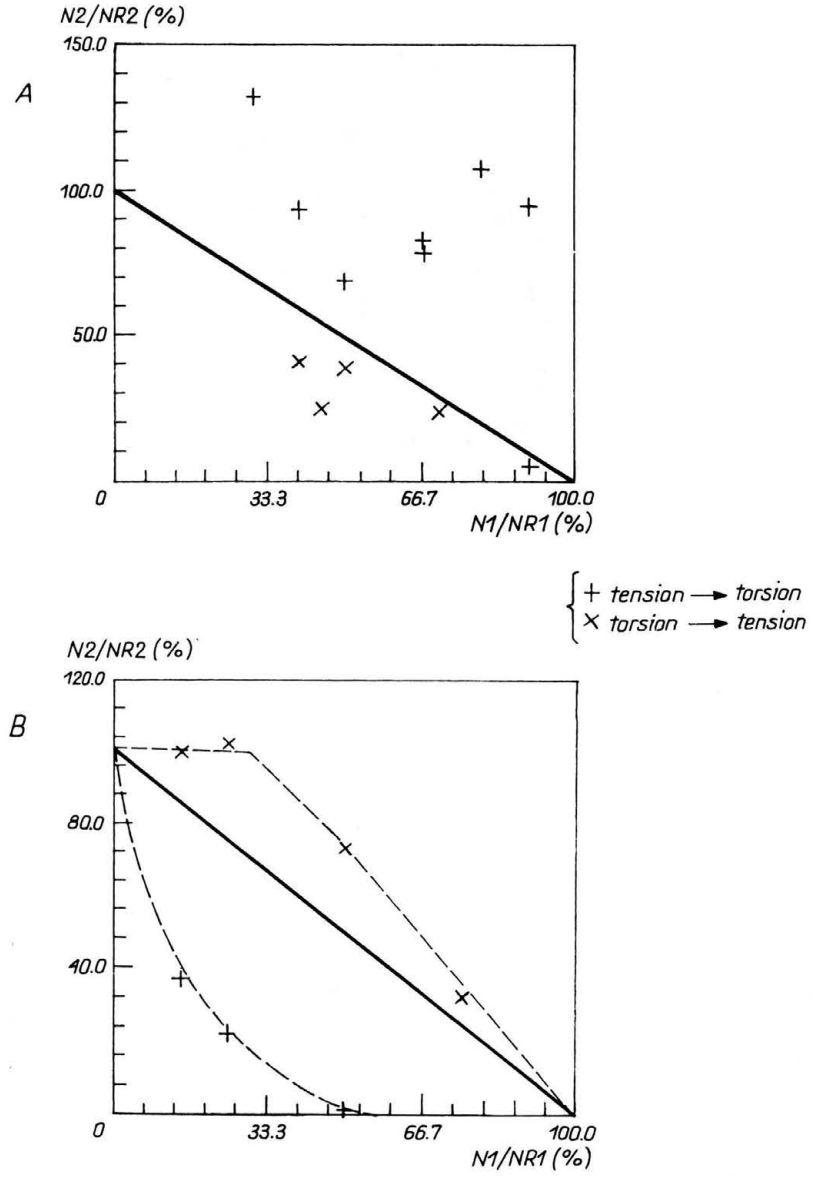

FIG. 16. Percentage of residual life as a function of the fraction of life already spent, during sequential tension and torsion tests carried out a) at 20°C in 12% chromium steel
b) at 600°C in 316 stainless steel.

Such history effects cannot be interpreted unless one considers the respective orientations of damage generated by each loading mode. Under tension-compression at room temperature cracks initiate at 45° to the tensile axis. These directions do not coincide neither with crack initiation, nor with crack propagation directions under reversed torsion at the strain level applied. That is why this damage is harmless under reversed torsion.

In the symmetric case, the transversal microcracks generated by torsion will not even have to branch to continue their extension under tension-compression. This damage is of course very efficient.

The fact that high temperature loading changes the crack initiation directions explains why the damage cumulation tendency is also reversed. Torsion damage (constituted by microcracks at 45° to the axis) is inefficient under tension-compression as long as a transversal macrocrack has not formed yet, whereas the transversal damage due to tension-compression is so detrimental under reversed torsion that there exists a critical crack density above which failure occurs immediately by instability.

These results illustrate the need of damage cumulation models that would take the orientation of cracks into account. An attempt to develop such a model was recently made by ROBILLARD and CAILLETAUD [5, 15]. They proposed to describe the damage occurring along each facet by an incremental law combining terms related to the shear and normal stress acting on it. This attempt was not completely successful, although it succeeded in reproducing the history effects in multiaxial damage cumulation quoted above.

The stumbling block for the development of such models is that damage evolution laws have to be assumed — or fitted — since very few experimental data exist on damage development kinetics, especially under reversed torsion. The development of in-situ experimental facilities should contribute to a better understanding of the damage process.

Acknowledgements

This work was carried out in the Ecole des Mines, in the laboratory of A. PINEAU who is gratefully acknowledged for his help and advice.

References

1. G. CAILLETAUD, R. KACZMAREK and B. POLICELLA, *Some elements of multiaxial behaviour of 316 stainless steel at room temperature*, Mech. Mat., **3**, 4, pp. 333–347, 1984.
2. B. JACQUELIN, F. BOURLIER and A. PINEAU, *Crack initiation under low cycle multiaxial fatigue*, ASTM STP, 853, Multiaxial Fatigue p. 285, 1985.
3. G. CAILLETAUD, V. DOQUET and A. PINEAU, *Prediction of macroscopic multiaxial behaviour from microstructural observations*, Proc. of 3rd Int. Conf. on Biaxial/Multiaxial Fatigue, April 3–6, Stuttgart 1989.
4. V. DOQUET, *Comportement et endommagement de deux aciers a structure C.C. et C.F.C. en fatigue oligocyclique sous chargement multiaxial non proportional*, Thesis, Ecole des Mines de Paris, June 23th, 1989.
5. M. ROBILLARD and G. CAILLETAUD, *Directionally defined damage in multiaxial low cycle fatigue: experimental evidence and tentative modelling*, Proc. 3rd Int. Conf. on Biaxial/Multiaxial Fatigue, April 3–6, Stuttgart 1989.
6. V. DOQUET and A. PINEAU, *Extra hardening due to cyclic non-proportional loading of an austenitic stainless steel*, Scripta Metall. Material., **24**, pp. 433–438, 1990.
7. V. DOQUET and A. PINEAU, *Multiaxial low cycle fatigue behaviour of a mild steel*, Proc. 3rd Int. Conf. on Biaxial/Multiaxial Fatigue, April 3–6, Stuttgart 1989.
8. J. BANNANTINE, D. F. SOCIE, *Observations of cracking behaviour in tension and torsion low cycle fatigue*, Low cycle fatigue ASTM STP, 942, Solomon, Halford, Kaisand and Lei Eds., pp. 899–921, Philadelphia 1988.
9. M. SAKANE, M. OHMANI and M. SAWADA, *Fracture modes and low cycle biaxial fatigue life at elevated temperature*, J. Eng. Mat. Techn., 109, pp. 236–243, July 1987.
10. T. HOSHIDE and D. F. SOCIE, *Crack nucleation and growth modelling in biaxial fatigue*, Eng. Fract. Mechn., **29**, 3, pp. 287–299, 1988.
11. D. SOCIE, C. T. HUA and D. W. WORTHEM, *Mixed mode small cracks growth*, Fat. Fract. Eng. Mat., Struct., 10, 1, pp. 1–16, 1987.

12. M. CLAVEL, P. PILVIN and R. RAHOUADJ, *Analyse microstructurale de la déformation plastique sous sollicitations non proportionelles dans un alliage base nickel*, Compte Rendu Acad. Sci. Paris, Serie II, 309, pp. 689–694, 1989.
13. L. C. LIM, *Surface intergranular cracking in large strain fatigue*, Acta Met., 35, 7, pp. 1653–1662, 1987.
14. S. MURAKAMI, M. KAWAI, K. AOKI and Y. OHMI, *Temperature dependence of multiaxial non-proportional cyclic behaviour of type 316 stainless steel*, J. Eng. Mat. Techn., 111, pp. 32–39, January 1989.
15. M. ROBILLARD, *Etude de l'endommagement et de la rupture en fatigue oligocyclique multiaxiale*, Thesis, Ecole des Mines de Paris, December 21th, 1989.

LABORATOIRE DE MECANIQUE DES SOLIDES
ECOLE POLYTECHNIQUE, PALAISEAU
AND
CENTRE DES MATERIAUX
ECOLES DES MINES, EVRY, FRANCE.

Received September 9, 1991.